Optimization of Waverider Configurations Generated from Axisymmetric Conical Flows

B.S. Kim,* M.L. Rasmussen,† and M.C. Jischke‡
The University of Oklahoma, Norman, Oklahoma

Analytic results from inviscid hypersonic small-disturbance theory for axisymmetric conical flow are used to generate waverider configurations valid for all values of $K_\delta \equiv M_\infty \delta$, where δ is the semivertex angle of the basic cone. By means of the calculus of variations, those configurations are sought that yield the maximum lift-to-drag ratio subject to suitable constraints, such as fixed lift, fixed volume, fixed base area, fixed planform area, and so on. The inviscid analysis accounts for wave drag only, but the effects of viscous drag are discussed. For the fixed-lift constraint, two types of optimized configurations are found: types with pointed noses, and types with round noses with sharp leading edges. The results are analytic in nature and particularly suitable for studying the various tradeoffs that are involved in missile design. Comparison of the results with other types of lifting bodies suggests that properly selected cone-derived waveriders are among the best producers of large lift-to-drag ratios.

Nomenclature

A_b = base area of waverider
D = drag
F_ℓ = integrand associated with lift
F_d = integrand associated with drag
F_g = integrand associated with constraint
G = constraint functional
H = optimizing functional with constraint
I_ℓ = integral associated with lift
I_d = integral associated with wave drag
I_g = integral associated with constraint
K_δ = hypersonic similarity parameter $= M_\infty \delta$, δ in radians
L = lift
ℓ = length of basic cone
M_∞ = freestream Mach number
q = $\rho_\infty V_\infty^2/2$
R = θ_b/δ
r = radial distance from vertex
S = projected planform area
S_B = area of shock-layer base plane
S_w = wetted area of waverider forebody
V_∞ = freestream velocity
V = volume of waverider
β = basic-shock semivertex angle
γ = ratio of specific heats
δ = basic-cone semivertex angle
$\tilde{\delta}$ = variational operator
ϕ = azimuthal angle, measured from x-z plane
ϕ_ℓ = azimuthal angle of waverider compression surface at the shock in the base plane, dihedral angle
ϕ_δ = azimuthal angle at intersection of winglet compression surface with basic-cone surface
ϕ_{lc} = critical dihedral angle, demarcation between class A and class B configurations
ϕ_{lo} = dihedral angle for fully optimized configuration
λ = Lagrange multiplier
σ = β/δ
θ = polar angle, measured from z axis
θ_b = polar angle of compression-surface trailing edge

Presented as Paper 82-1299 at the AIAA 9th Atmospheric Flight Mechanics Conference, San Diego, Calif., Aug. 9-11, 1982; submitted Aug. 9, 1982; revision received Feb. 20, 1983.

*Graduate Student, Aerospace, Mechanical, and Nuclear Engineering.
†Professor, Aerospace, Mechanical, and Nuclear Engineering. Associate Fellow AIAA.
‡Dean, College of Engineering. Associate Fellow AIAA.

Introduction

NONCIRCULAR body cross sections and various lifting-body configurations are of current interest as a means for obtaining high-performance supersonic missile characteristics. Although the use of digital computers greatly facilitates the calculation of general three-dimensional hypersonic flows, the complexity and expense of these calculations do not lend themselves to parametric studies or the basic understanding desirable for missile design considerations. Thus special configurations from which the flowfields are simple and well known become particularly suitable for delineating various tradeoffs that are involved in missile design. A class of lifting-body configurations that is particularly suitable for fundamental study is that of waveriders derived from supersonic conical flows.

The notion of using stream surfaces of known flowfields to develop waverider configurations is well established.[1-5] A general discussion of waverider aerodynamics is given by Küchemann.[6] These ideas have been extended to use the flowfields of slightly inclined, nearly circular cones.[7,8]

While such results are very useful, there are an infinite number of possibilities for such waverider configurations. The problems of missile design are concerned with possible optimized configurations. This paper discusses optimization of waverider configurations derived from axisymmetric conical flowfields with the aim of generalizing the analysis to nonaxisymmetric flowfields. The specific problem is to maximize the inviscid lift-to-drag ratio of cone-derived waveriders when such factors as lift, cone angle, Mach number, body volume, base area, and planform area are used as constraints. The approach is akin to that of Cole and Zien,[5] but the analysis is generalized and accurate flowfield approximations[7] are used to generate simple analytic results.

Most previous works dealing with optimization of configurations in hypersonic flow have assumed the surface pressures to be given by Newtonian theory. Pertinent examples are those of Lusty and Miele[9] and Huang.[10] At best these works are applicable strictly to the limit when $K_\delta \equiv M_\infty \delta$ tends to infinity, where δ is a pertinent flow-deflection angle.

Further, the flowfield structure and shock shape are not accounted for as part of the analysis. In the present study, the analysis lies within the framework of inviscid hypersonic small-disturbance theory, and the results are valid for arbitrary values of the similarity parameter K_δ. In addition, the flowfield and shock shape are known for the on-design conditions of the optimized waveriders.

The detailed results presented herein are for a lift-fixed constraint, but the methodology is directly applicable to other constraints that are suggested. Comparison of the results with other lifting-body configurations is also given, along with an estimate of viscous-drag effects.

Formulation of the Problem

General Results

The forces acting on a body in steady supersonic flow are determined here by means of the integral equations of inviscid gasdynamics. Consider a Cartesian coordinate system such as shown in Fig. 1, with the freestream velocity V_∞ pointing in the positive z direction. We assume that a waverider configuration is comprised of three surfaces: a compression stream surface, a freestream surface that intersects the compression stream surface on the shock, and a base-plane surface perpendicular to the freestream, located at $z=\ell$. The base pressure is assumed equal to the freestream pressure, $p_b=p_\infty$, which is tantamount to omitting the base drag in the ensuing analysis.

Let the shock-layer region upstream of the base be enclosed by a combination of three surfaces: a surface embracing the freestream side of the shock, the stream surface constituting the compression surface on the waverider (which intersects the shock), and a shock-layer base plane perpendicular to the freestream at $z=\ell$ which is intersected by the shock surface and the compression stream surface. Since $p=p_\infty$ on the freestream side of the shock surface as well as the freestream surface and base plane of the waverider, and $\vec{V}\cdot\hat{n}=0$ on the compression surface, the force on the waverider stemming from the excess pressure on the compression surface can be converted entirely to an integral over the shock-layer base plane by means of the mass and momentum integral equations from steady inviscid gasdynamics. Thus the force on the waverider can be written

$$F=-\int_{S_B}\int [(p-p_\infty)\hat{e}_z+\rho(V-V_\infty)V\cdot\hat{e}_z]\,dS \tag{1}$$

where S_B is the area of the shock-layer base plane, $\hat{e}_z$ the unit vector pointing in the positive z direction, p the pressure, ρ the density, and V the fluid velocity.

We assume that the flow is symmetric about the x-z plane such that the side forces in the $\hat{e}_y$ direction vanish. The force vector can thus be resolved into a lift component in the negative $\hat{e}_x$ direction and a wave-drag component in the $\hat{e}_z$ direction:

$$L\equiv -F\cdot e_x=\int_{S_B}\int \rho(V\cdot\hat{e}_x)(V\cdot\hat{e}_z)\,dS \tag{2}$$

$$D_w\equiv F\cdot\hat{e}_z=-\int_{S_B}\int [p-p_\infty+\rho\{V\cdot\hat{e}_z-V_\infty\}(V\cdot\hat{e}_z)]\,dS \tag{3}$$

Axisymmetric Conical Flow

Consider now a spherical coordinate system with r the distance along a ray from the origin, θ the polar angle measured from the z axis, and ϕ the azimuthal angle measured from the x-z plane. For steady axisymmetric conical flow, all the flow variables depend only on θ, and the velocity vector has the form

$$V=u(\theta)\hat{e}_r+v(\theta)\hat{e}_\theta=\hat{e}_x(u\sin\theta+v\cos\theta)\cos\phi$$
$$+\hat{e}_y(u\sin\theta+v\cos\theta)\sin\phi+\hat{e}_z(u\cos\theta-v\sin\theta) \tag{4}$$

Thus the expressions for lift and wave drag become

$$L=\int_{S_B}\int \rho(u\sin\theta+v\cos\theta)(u\cos\theta-v\sin\theta)\cos\phi\,dS \tag{5}$$

$$D_w=-\int_{S_B}\int [p-p_\infty+\rho(u\cos\theta-v\sin\theta$$
$$-V_\infty)(u\cos\theta-v\sin\theta)]\,dS \tag{6}$$

Hypersonic Small-Disturbance Approximations

Consider the flowfield generated by slender cones at large Mach numbers such that $\sin\theta\simeq\theta$, $\cos\theta\simeq 1$, and δ and β are the semivertex angles of the cone body and shock. We consider the limit such that $K_\delta\equiv M_\infty\delta$ is fixed when $\delta\to 0$ and $M_\infty\to\infty$. As for other problems that have led to accurate results,[7,11-13] we assume the approximate formulas

$$u(\theta)\simeq V_\infty\left[1-\frac{\delta^2}{2}\left(\frac{\theta^2}{\delta^2}+\ell n\frac{\beta^2}{\theta^2}\right)\right] \tag{7a}$$

$$v(\theta)\simeq -V_\infty\theta\left(1-\frac{\delta^2}{\theta^2}\right) \tag{7b}$$

$$\frac{T(\theta)}{T_\infty}\simeq 1+\frac{\gamma-1}{2}K_\delta^2\left[2-\frac{\delta^2}{\theta^2}+\ell n\frac{\beta^2}{\theta^2}\right] \tag{7c}$$

$$\frac{p(\theta)}{p_\infty}\simeq 1+\frac{\gamma}{2}K_\delta^2\left[1+\frac{\rho(\beta)}{\rho_\infty}\left(1-\frac{\delta^2}{\theta^2}+\ell n\frac{\beta^2}{\theta^2}\right)\right] \tag{7d}$$

$$\frac{\rho(\theta)}{\rho_\infty}=\frac{p(\theta)/p_\infty}{T(\theta)/T_\infty}\simeq\frac{\rho(\beta)}{\rho_\infty}\left[1+\frac{K_\delta^2}{2[T(\beta)/T_\infty]}\right.$$
$$\left.\times\left(\frac{\delta^2}{\beta^2}-\frac{\delta^2}{\theta^2}+\ell n\frac{\beta^2}{\theta^2}\right)\right] \tag{7e}$$

where

$$\frac{\rho(\beta)}{\rho_\infty}\equiv\frac{\sigma^2}{\sigma^2-1} \tag{7f}$$

and

$$\sigma\equiv\frac{\beta}{\delta}\simeq\left[\frac{\gamma+1}{2}+\frac{1}{K_\delta^2}\right]^{1/2} \tag{7g}$$

The surface area element is approximately $dS=\ell^2\theta\,d\theta\,d\phi$, where ℓ is the length of the cone.

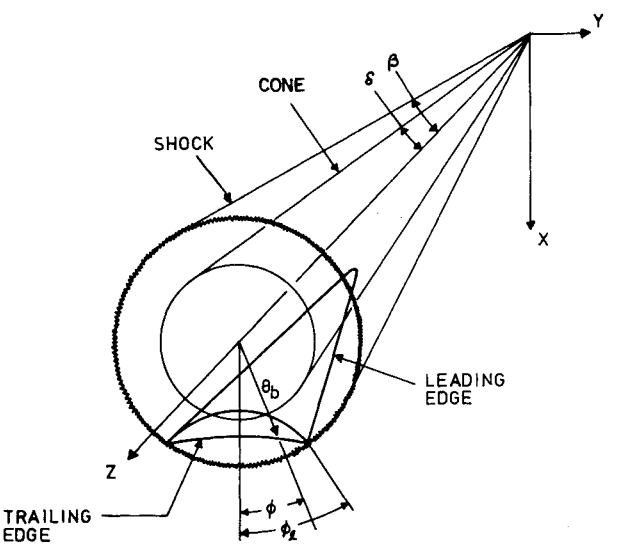

Fig. 1 Geometric configuration and coordinate system.

To lowest order in δ the lift and drag integrals can now be written

$$L=4q\ell^2\delta^2\int_0^{\phi_\ell}\int_{\theta_b}^{\beta}\frac{\rho}{\rho_\infty}\cos\phi\,d\theta\,d\phi \tag{8}$$

$$D=2q\ell^2\delta^2\int_0^{\phi_\ell}\int_{\theta_b}^{\beta}\left[\frac{\rho}{\rho_\infty}\left(2+\ell n\frac{\beta^2}{\theta^2}\right)-\frac{C_p}{\delta^2}\right]\theta\,d\theta\,d\phi \tag{9}$$

where

$$\frac{C_p(\theta)}{\delta^2}=1+\frac{\rho(\beta)}{\rho_\infty}\left(1-\frac{\delta^2}{\theta^2}+\ell n\frac{\beta^2}{\theta^2}\right) \tag{10}$$

and $q\equiv\rho_\infty V_\infty^2/2$, $\theta_b(\phi)$ is the polar angle of the trailing edge of the compression stream surface in the base plane, and ϕ_ℓ is the azimuthal angle in the base plane where the compression stream surface intersects the shock. The variation in density across the shock layer is small and makes an insignificant contribution to the value of L and D. Therefore we set $\rho(\theta)=\rho(\beta)$ inside the integrals [which is consistent with the original derivation of Eqs. (7)], carry out the integrations over θ, and write the lift and wave drag as

$$L=q\ell^2\delta^3\left(\frac{4\sigma^3}{\sigma^2-1}\right)\int_0^{\phi_\ell}\left[1-\frac{R(\phi)}{\sigma}\right]\cos\phi\,d\phi \tag{11}$$

$$D_w=q\ell^2\delta^4\left(\frac{\sigma^2}{\sigma^2-1}\right)\int_0^{\phi_\ell}\left[1-\frac{R^2(\phi)}{\sigma^2}-\ell n\frac{R^2(\phi)}{\sigma^2}\right]d\phi \tag{12}$$

where

$$R(\phi)\equiv\frac{\theta_b(\phi)}{\delta} \tag{13}$$

is, at this stage, an arbitrary function describing the trailing edge of the compression surface in the base plane. When $R(\phi)$ and ϕ_ℓ are specified, the lift and drag can be calculated.

The Compression Stream Surface

The streamlines in the shock layer are described by the equation $V+ds=0$. From this equation it can be established that one family of arbitrary stream surfaces can be described by

$$r\left[\frac{\rho(\theta)v(\theta)\sin\theta}{\rho(\beta)v(\beta)\sin\beta}\right]^{1/2}=r_s(\phi) \tag{14a}$$

where $r_s(\phi)$ is an arbitrary function of ϕ. It is useful to interpret $r_s(\phi)$ as an arbitrary line drawn on the shock surface, and thus Eq. (14a) describes the shock-layer stream surface starting on the line $r=r_s(\phi)$. The approximation consistent with the previous section is

$$r\left[\frac{\theta^2-\delta^2}{\beta^2-\delta^2}\right]^{1/2}=r_s(\phi) \tag{14b}$$

The function $r_s(\phi)$ can also be determined in terms of the function $R(\phi)$ for the trailing edge of the compression surface in the base plane. Setting $\theta=\theta_b(\phi)$ when $r=\ell\sec\theta_b\simeq\ell$, we obtain

$$r_s(\phi)\equiv\ell\left[\frac{R^2(\phi)-1}{\sigma^2-1}\right]^{1/2} \tag{15}$$

Thus, when $R(\phi)$ is specified, the intersection of the compression stream surface with the shock is determined, along with the complete compression stream surface itself from Eq. (14b).

The Waverider Freestream Surface

An arbitrary cylindrical surface parallel to the freestream can be expressed as $r\sin\theta=f(\phi)$, where $f(\phi)$ is an arbitrary function of ϕ. Thus, for small angles, the freestream surface intersecting the shock at $r_s(\phi)$ is given by

$$r\frac{\theta}{\beta}=r_s(\phi)\equiv\ell\left[\frac{R^2(\phi)-1}{\sigma^2-1}\right]^{1/2} \tag{16}$$

Correspondingly, the trailing edge of the freestream surface in the base plane is given by

$$\frac{\theta_{fs}(\phi)}{\delta}=\sigma\left[\frac{R^2(\phi)-1}{\sigma^2-1}\right]^{1/2} \tag{17}$$

Thus, when $R(\phi)$ is specified, the complete shape of the waverider can be determined, as well as the lift and drag.

Geometric Variables

When the shape of the waverider is known as a function of $R(\phi)$, other variables of interest can be determined. Among the variables of particular interest are the base area of the waverider A_b, the volume V, the planform area S (projected onto the y-z plane), and the wetted area of the forebody S_w. These variables can be determined by the following integrals:

$$A_b=\ell^2\delta^2\int_0^{\phi_\ell}\left[1-\frac{R^2-1}{\sigma^2-1}\right]d\phi \tag{18}$$

$$V=\ell^3\delta^2\int_0^{\phi_\ell}\left[\frac{1}{3}-\frac{R^2-1}{\sigma^2-1}+\frac{2}{3}\left(\frac{R^2-1}{\sigma^2-1}\right)^{3/2}\right]d\phi \tag{19}$$

$$S=\frac{2\ell^2\delta\sigma}{\sigma^2-1}\int_0^{\phi_\ell}RR'\sin\phi\,d\phi \tag{20}$$

$$S_w=2\ell^2\delta\int_0^{\phi_\ell}[s_{fs}+s_c]\,d\phi \tag{21}$$

where

$$s_{fs}=\frac{\sigma}{\sqrt{\sigma^2-1}}\left[1-\sqrt{\frac{R^2-1}{\sigma^2-1}}\right]\sqrt{(R^2-1)+\frac{(RR')^2}{R^2-1}} \tag{22}$$

$$s_c=\int_a^1\sqrt{x^2+R^2-1+\frac{(RR')^2}{x^2+R^2-1}}\,dx$$

$$a\equiv\sqrt{\frac{R^2-1}{\sigma^2-1}} \tag{23}$$

The functions s_{fs} and s_c pertain to the wetted areas of the freestream and compression surfaces. As for the lift and drag, these integrals are functionals involving the function $R(\phi)$.

The Optimization Problem

Maximum Lift-to-Drag Ratio

We consider the variational problem of finding the compression-surface trailing-edge function $R(\phi)$ such that the inviscid lift-to-drag ratio is a maximum:

$$\frac{L}{D_w}=\frac{4\sigma}{\delta}\frac{I_\ell}{I_d} \tag{24}$$

Here, I_ℓ and I_d are the functionals

$$I_\ell\equiv\int_0^{\phi_\ell}F_\ell(R,\phi;\sigma)\,d\phi \tag{25a}$$

$$I_d\equiv\int_0^{\phi_\ell}F_d(R,\phi;\sigma)\,d\phi \tag{25b}$$

and the integrands are

$$F_\ell(R,\phi;\sigma)\equiv\left(1-\frac{R}{\sigma}\right)\cos\phi \tag{26a}$$

$$F_d(R,\phi;\sigma)\equiv 1-\frac{R^2}{\sigma^2}-\ell n\frac{R^2}{\sigma^2} \tag{26b}$$

The maximum of the L/D ratio is to be found subject to a constraint of the form

$$G(R',R,\phi;q,\ell,\delta,\sigma) \equiv g(q,\ell,\delta,\sigma) I_g = k \tag{27a}$$

where k is a constant, and I_g is a functional of the form

$$I_g \equiv \int_0^{\phi_\ell} F_g(R',R,\phi;\sigma)\,\mathrm{d}\phi \tag{27b}$$

Any one of the expressions for L, A_b, V, S, or S_w could be used as a special case of the constraint function. Thus the maximum of L/D_w is to be found such that some functional such as L, A_b, V, S, or S_w is held fixed.

Besides the function $R(\phi)$ to be varied, along with the endpoint ϕ_ℓ, there are other parameters in the constraint function G that could be varied. In particular we shall be interested additionally in the variation of the basic-cone angle δ, where the other parameters in the problem q, ℓ, and M_∞ are to be considered fixed.

The Variational Problem

To accommodate the constraint condition in the variational analysis, we introduce the Lagrange multiplier λ and consider the functional H:

$$H \equiv L/D_w - \lambda G \tag{28}$$

The ensuing analysis is now akin to standard problems of isoperimetric form.[14,15] In addition, we impose the additional inequality constraint that the stream-surface trailing-edge function $R(\phi)$ lie in the shock layer, that is,

$$1 \le R(\phi) \le \sigma \tag{29}$$

The optimizing of the functional H with regards to $R(\phi)$ and the variable end conditions $R(\phi_\ell) = \sigma$ is accounted for by the variational operation§

$$\delta H = 0 \tag{30}$$

At this stage, the configuration is said to be *semioptimized.* In addition, we wish to vary δ and hold the other variables q, ℓ, and M_∞ fixed. Hence, we have also

$$\frac{\partial H}{\partial \delta} = 0 \tag{31}$$

After the final imposition of condition (31), the configuration is said to be *fully optimized.*

The variational operation (30) leads to

$$\delta H \equiv \frac{4}{\delta}\frac{\sigma}{I_d}\left[\delta I_\ell - \frac{I_\ell}{I_d}\delta I_d - \frac{\lambda g I_d}{(4\sigma/\delta)}\delta I_g\right] = 0 \tag{32}$$

Since F_ℓ and F_d do not depend on R', the vanishing of the terms in brackets leads to the Euler-Lagrange equation:

$$\frac{\partial F_\ell}{\partial R} - \frac{I_\ell}{I_d}\frac{\partial F_d}{\partial R} - \frac{\lambda g I_d}{(4\sigma/\delta)}\left[\frac{\partial F_g}{\partial R} - \frac{\mathrm{d}}{\mathrm{d}\phi}\left(\frac{\partial F_g}{\partial R'}\right)\right] = 0 \tag{33}$$

The variable end conditions $R(\phi_\ell) = \sigma$ is governed by the transversality condition[14,15]

$$\left[F_\ell - \frac{I_\ell}{I_d}F_d - \frac{\lambda g I_d}{(4\sigma/\delta)}\left\{F_g - R'\frac{\partial F_g}{\partial R'}\right\}\right]_{\phi=\phi_\ell} = 0 \tag{34}$$

which for the constraint function represented by L, A_b, V, S, or S_w is satisfied identically. The derivative (31) is to be evaluated with λ held constant.

Lift-Fixed Constraint

For the constraint of fixed lift, we set $G = L$ and hence $g = q\ell^2\delta^3 4\sigma^3/(\sigma^2 - 1)$ and $F_g = F_\ell$. For this case, the problem also can be interpreted as finding the minimum-drag configuration for a fixed amount of lift. The Euler-Lagrange equation (33) can be written

$$\frac{\partial}{\partial R}(F_\ell - \lambda^* F_d) = 0 \tag{35}$$

where

$$\lambda^* \equiv \frac{I_\ell/I_d}{1 - [\lambda g I_d/(4\sigma/\delta)]} \tag{36}$$

The solution to the problem is obtained by taking the partial derivative with respect to R and then solving the resulting equation for $R(\phi)$. Enforcing the boundary condition $R(\phi_\ell) = \sigma$ leads to the value for λ^*, and the results are

$$\lambda^* = \cos\phi_\ell/4 \tag{37}$$

$$R(\phi) = \frac{\sigma}{\cos\phi_\ell}\left[\cos\phi - \sqrt{\cos^2\phi - \cos^2\phi_\ell}\right] \tag{38}$$

For certain values of ϕ_ℓ and σ, the function (38) cannot satisfy the constraint (29) for all values of ϕ in the range $0 \le \phi \le \phi_\ell$. The cases where $R(\phi) < 1$ are not permissible since a shock-layer stream surface cannot lie inside the surface of the basic cone itself. It thus transpires that there are two classes of solutions: one in which the function (38) is valid for all ϕ in the range $0 \le \phi \le \phi_\ell$; and one in which the function (38) defines winglets in the regime $\phi_\delta \le \phi \le \phi_\ell$, where $R(\phi_\delta) = 1$, and the remaining part of the stream surface in the range of $0 \le \phi \le \phi_\delta$ is the surface of the basic cone itself. The latter is referred to as class A and the former as class B.

The critical value of ϕ_ℓ, say $\phi_{\ell c}$, occurs when $R(0) = 1$, which is determined from Eq. (38) to be

$$\sin\phi_{\ell c} = (\sigma^2 - 1)/(\sigma^2 + 1) \tag{39}$$

When ϕ_ℓ is greater than $\phi_{\ell c}$, the solution will be of class A, whereas the solution will be of class B when $\phi_\ell < \phi_{\ell c}$. The critical value of the dihedral angle $\phi_{\ell c}$ is shown in Fig. 2 as a function of $K_\delta \equiv M_\infty \delta$. In the hypersonic limit $K_\delta \to \infty$, the critical dihedral angle tends to $\phi_{\ell c} \to 5.2$ deg, for $\gamma = 1.4$, whereas in the linearized-theory limit $K_\delta \to 0$, $\phi_{\ell c} \to 90$ deg. When $K_\delta = 1$, then $\phi_{\ell c} \simeq 22$ deg.

For the class A configurations the winglets intersect the basic cone (at the base) at ϕ_δ, which is determined from Eq. (38) from the condition $R(\phi_\delta) = 1$:

$$\cos\phi_\delta = \cos\phi_\ell/\cos\phi_{\ell c} \qquad \phi_\ell \ge \phi_{\ell c} \tag{40}$$

Examples of the semioptimized waverider base shapes are shown in Figs. 3a, 3b, and 3c for $K_\delta = 0.5$, 1, and 5, respectively. For each K_δ there are shown class A shapes for $\phi_\ell > \phi_{\ell c}$ and class B shapes for $\phi_\ell < \phi_{\ell c}$. The class A shapes have pointed noses since streamlines on the surface of the basic cone originate at the vertex, and the class B shapes have round noses with sharp lips since streamlines in the shock layer originate at some point on the basic-shock surface. Figure 4 shows the end views, top views, and side views of the two classes of waveriders for $K_\delta = 1$. The freestream surfaces are determined by means of Eq. (17). The class B shapes are not conical since the cross-section shapes are not similar as z varies, as can be seen from Eq. (14b). The winglets on the class A shapes also are not conical, although the cone segment of the compression surface for $0 \le \phi \le \phi_\delta$, of course, is conical since it is part of the original basic cone. The fully optimized configurations are denoted by $\phi_\ell = \phi_{\ell o}$.

§Here, the variational operator δ should not be confused with the basic-cone angle δ.

When Eq. (31) is enforced, the semioptimized shapes are restricted by a relation between ϕ_ℓ and $K_\delta \equiv M_\infty \delta$, which gives the fully optimized dihedral angle $\phi_{\ell o}$. Performing the differentiation $\partial H/\partial\delta$ and accounting for $4\lambda^* = \cos\phi_\ell$ lead to the equation

$$\frac{4}{\cos\phi_{\ell o}}\frac{I_\ell}{I_d} = \left(4\sigma^2 K_\delta^2 + \frac{2}{\sigma^2-1} - \frac{\sigma}{I_d}\frac{\partial I_d}{\partial\sigma}\right) \Big/ \left(3\sigma^2 K_\delta^2 - \frac{\sigma^2-3}{\sigma^2-1} - \frac{\sigma}{I_\ell}\frac{\partial I_\ell}{\partial\sigma}\right) \tag{41}$$

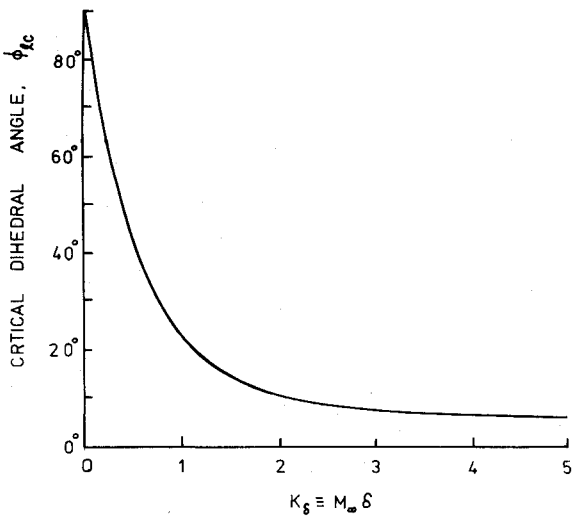

Fig. 2 Critical dihedral angle for semioptimized waveriders.

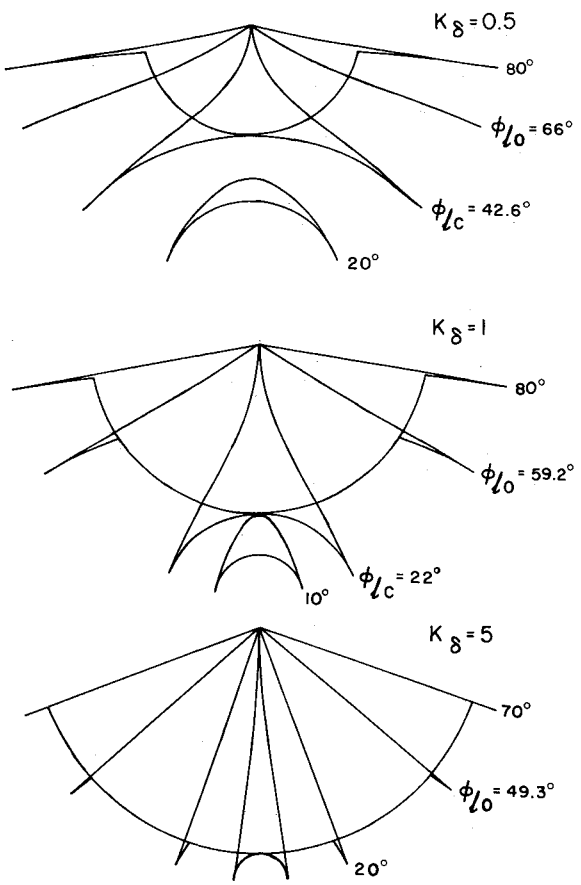

Fig. 3 Semioptimized waverider base shapes. a) $K_\delta = 0.5$, b) $K_\delta = 1$, c) $K_\delta = 5$.

where

$$\frac{\partial I_\ell}{\partial\sigma} = 0 \qquad \text{class B}$$

$$= \frac{\sin\phi_\delta}{\sigma^2} \qquad \text{class A}$$

$$\frac{\partial I_d}{\partial\sigma} = 0 \qquad \text{class B}$$

$$= \frac{2(1+\sigma^2)}{\sigma^3}\phi_\delta \qquad \text{class A}$$

For class A bodies the integrals I_ℓ and I_d depend both on ϕ_ℓ and σ, whereas for the class B bodies they depend only on ϕ_ℓ. The relations between $\phi_{\ell o}$ and K_δ generated by Eq. (41) are shown in Fig. 5. For small K_δ, the fully optimized lift-fixed bodies are of class B, and $\phi_{\ell o} \to 72.3$ deg as $K_\delta \to 0$. As K_δ increases above $K_\delta \simeq 0.17$, the fully optimized bodies are of class A, and $\phi_{\ell o} \to 49$ deg as $K_\delta \to \infty$. This asymptotic hypersonic-limit result is in close agreement with the numerical result of Cole and Zien[5] for $K_\delta = \infty$, which demonstrates the accuracy of the present analysis.

Idealized Cone Waverider

As a basis for comparison with the optimized waveriders, it is useful to consider a simple configuration that is a special case of the nonoptimized configurations and is easy to visualize. This idealized waverider[16] is conical in shape with infinitesimally thin delta winglets, as illustrated in Fig. 6. The particular results for all the variables come from setting $R(\phi) \equiv 1$ in all the integrals. We then get

$$L = q\,\ell^2\delta^3\,[4\sigma^2/(\sigma+1)]\sin\phi_\ell \tag{42a}$$

$$D_w = q\,\ell^2\delta^2 C_p(\delta)\,\phi_\ell \tag{42b}$$

where $C_p(\delta)$ is determined from Eq. (10). In addition, we have $V^* = \ell A_b^*/3 = \ell^3\delta^2\phi_\ell/3$; $S^* = \ell^2\delta\sigma\,\sin\phi_\ell$; and $S_w^* = \ell^2\delta(2\sigma - 1 + \phi_\ell)$. The idealized cone waverider yields nearly the same

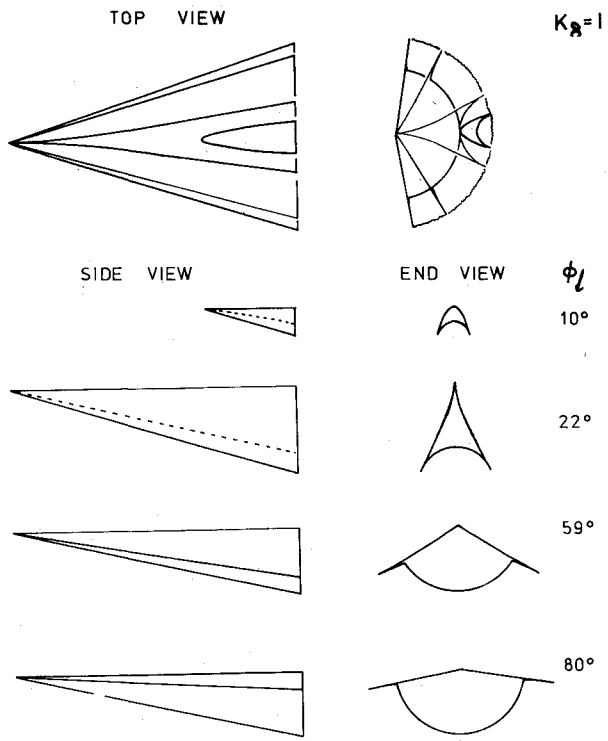

Fig. 4 End views, top views, and side views of semioptimized waveriders for $K_\delta = 1$.

results as the optimized class A configuration in the limit $K_\delta \to \infty$. For the idealized cone waverider, the optimization problem corresponding to Eqs. (30) and (31) reduces to $\partial H/\partial\phi_\ell = 0$ and $\partial H/\partial\delta = 0$.

Performance of Optimized Waveriders for Fixed-Lift Constraint

Basic Results

The fixed-lift constraint problem corresponds to finding the minimum-drag configuration for a given lift. For the semioptimized configurations (that is, δ held fixed and only $R(\phi)$ and ϕ_ℓ varied), the dihedral angle ϕ_ℓ can be eliminated between lift and drag so that $D/q\ell^2\delta^4\sigma$ can be plotted as a function of $L/q\ell^2\delta^3\sigma$ with K_δ used as a parameter, as shown in Fig. 7. For a given lift, and q, ℓ, δ, and σ held fixed, the drag for the idealized cone waverider is always greater than the semioptimized shape. This, of course, would also be true for any arbitrary waverider formed in the shock layer of a given cone for q, ℓ, δ, and σ held fixed. The idealized cone waverider is a good approximation to the semioptimum shapes when K_δ is greater than unity. The origin of the curves in Fig. 7 corresponds to $\phi_\ell = 0$; the end of the curves corresponds to $\phi_\ell = 90$ deg; and the solid-circle point represents the location of $\phi_{\ell c}$.

Figure 8 shows the ratio $(L\delta)/(D\sigma)$ as a function of ϕ_ℓ for various values of K_δ for the semioptimized bodies. All the curves for various values of K_δ stem from a common curve, the point of tangential departure being $\phi_{\ell c}$ and denoted by a circle. For a given ϕ_ℓ, the ratio $(L\delta)/(D\sigma)$ increases as K_δ increases. The dashed curves for the idealized cone waverider for $K_\delta = 0.1$ and 0.5 give smaller values of $(L\delta)/(D\sigma)$ than the corresponding semioptimized configurations, as should be expected, but the idealized cone waverider gives a better approximation for larger values of K_δ, being nearly indistinguishable from the semioptimized configurations at $K_\delta = \infty$. For a given value of K_δ, the class B waveriders have larger values of $(L\delta)/(D\sigma)$.

The fully optimized (δ varied) values of $(L\delta)/(D\sigma)$ are shown in Fig. 9 as a function of K_δ, together with the corresponding fully optimized results for the idealized cone waverider. For larger values of K_δ, the two results become closer. Note that since σ becomes larger as K_δ becomes smaller, the actual value of $L\delta/D$ tends to increase as K_δ becomes smaller. The circle shows the location of $\phi_{\ell c}$, which separates the class B (small K_δ) from the class A (large K_δ) configurations.

Figure 10 shows the actual values of L/D_w for the fully optimized waverider configurations as a function of δ for $M_\infty = 3$, 4, 5, and 6. These curves represent the class A configurations, since the class B configurations correspond to large L/D_w and small δ and are thus off the scale of Fig. 10. For a fixed value of δ, the values of L/D_w decrease as M_∞ increases. The solid circle data point represents the experimental result for the on-design elliptic-cone waverider of Ref. 17 ($M_\infty = 4$, $\delta = 18.6$ deg), which is slightly under the curve for $M_\infty = 4$ for the fully optimized waverider. The square data point represents the experimental result for the conical lifting body of Schindel[18] ($M_\infty = 6$, $\delta \simeq 13$ deg), which produces a smaller L/D than the fully optimized waveriders. The experimental results include the friction drag on the forebody.

Results in Terms of V, A_b, and S

It is desirable to express the results in a form appropriate for general comparison with other lifting-body configurations. This can be accomplished by means of the volume V, base area A_b, and projected planform area S, which are pertinent variables of interest in missile design. The volume for the semioptimized configurations, ratioed with the corresponding value V^* for the idealized cone waverider, is shown in Fig. 11 as a function of dihedral angle ϕ_ℓ for various values of K_δ. For large values of K_δ the idealized cone waverider provides a good approximation for the semioptimized configurations, except for small dihedral angles ϕ_ℓ.

Out of the dimensional variables V, A_b, and S there are two independent dimensionless combinations. One combination is $V^{2/3}/S$, which can be regarded as a measure of volume; and another combination is A_b/S, which can be regarded as a measure of slenderness. For the semioptimized configurations

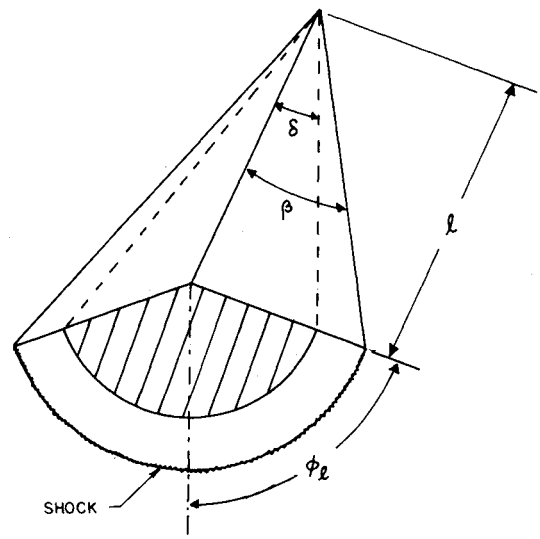

Fig. 6 Idealized cone waverider.

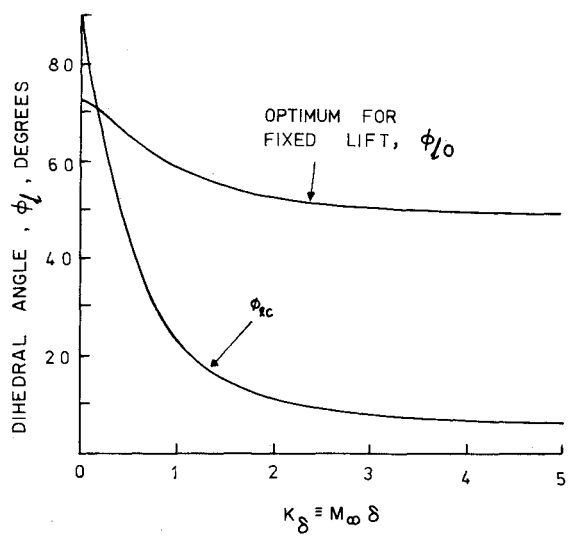

Fig. 5 Dihedral angle for fully optimized waveriders.

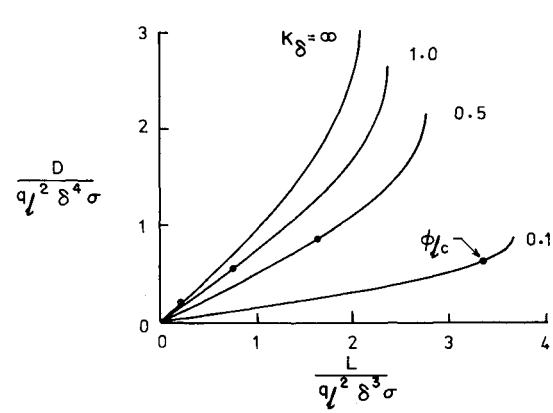

Fig. 7 Drag as a function of lift for semioptimized waveriders.

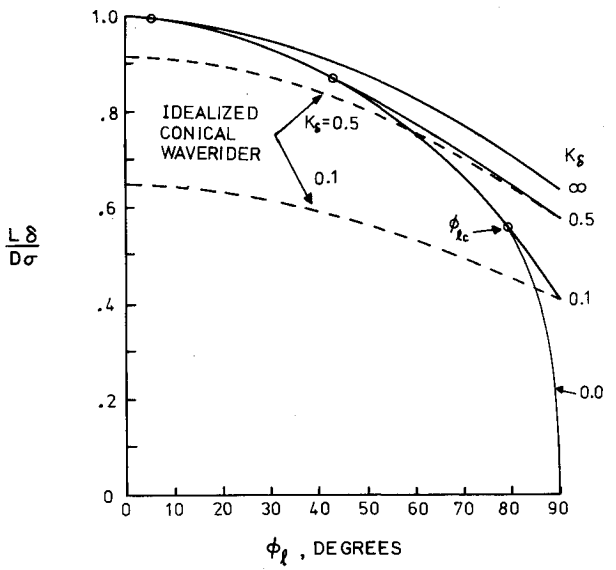

Fig. 8 Lift-to-drag ratio as a function of dihedral angle for semioptimized waveriders.

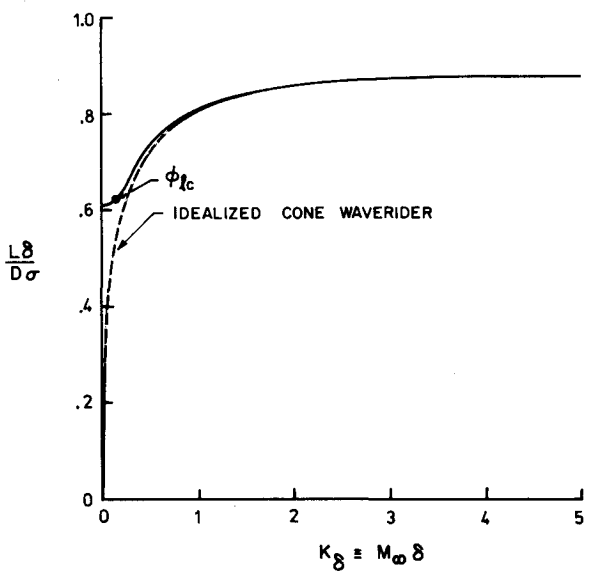

Fig. 9 Lift-to-drag ratio as a function of K_δ for fully optimized waveriders.

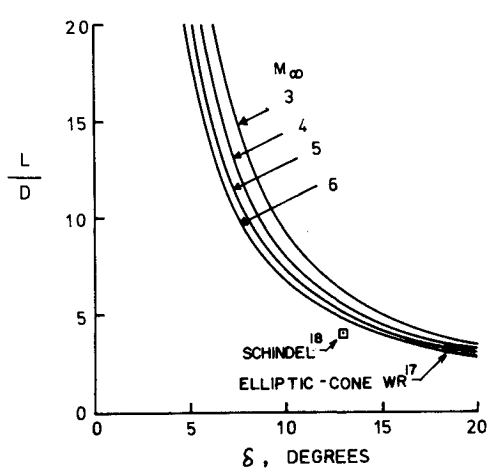

Fig. 10 Lift-to-drag ratio as a function of cone angle for fully optimized waveriders.

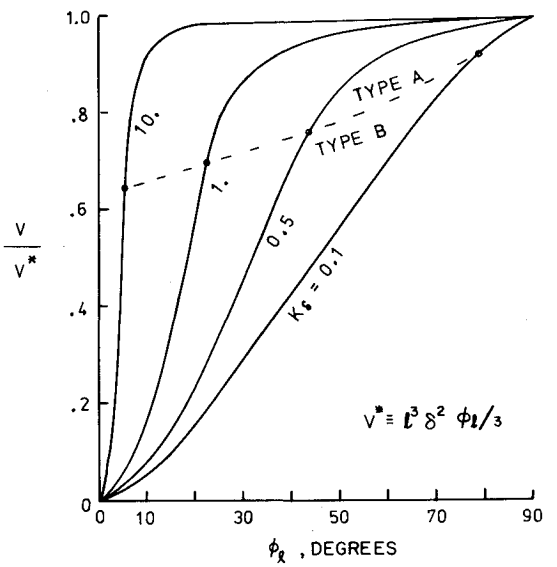

Fig. 11 Volume of semioptimized waveriders as a function of dihedral angle.

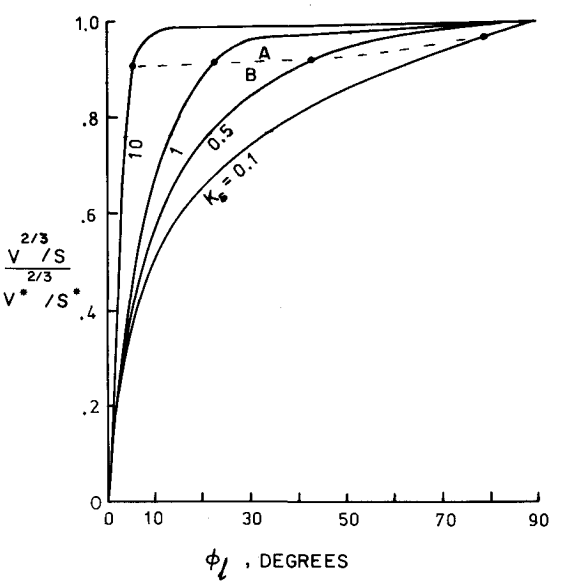

Fig. 12 Volume ratio for semioptimized waveriders as a function of dihedral angle.

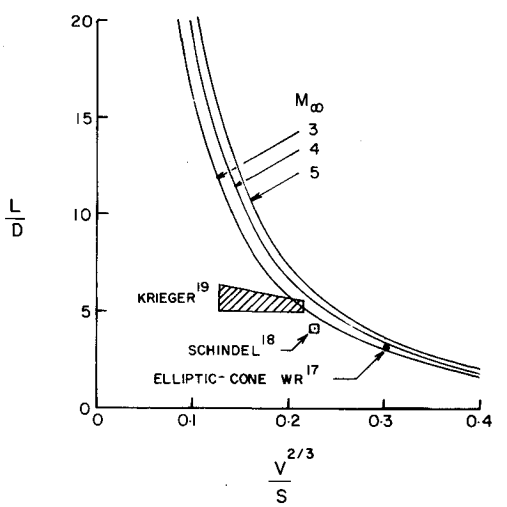

Fig. 13 Lift-to-drag ratio of fully optimized waveriders as a function of volume ratio.

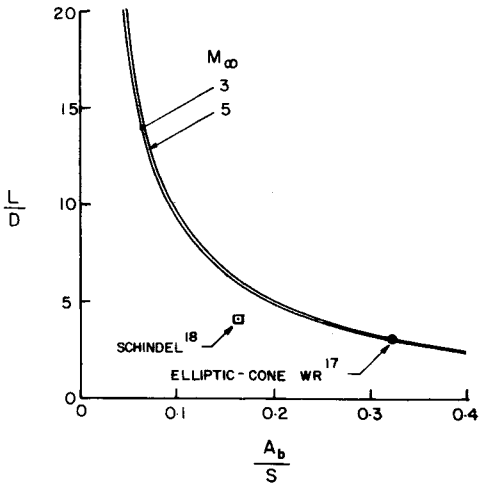

Fig. 14 Lift-to-drag ratio of fully optimized waveriders as a function of slenderness ratio.

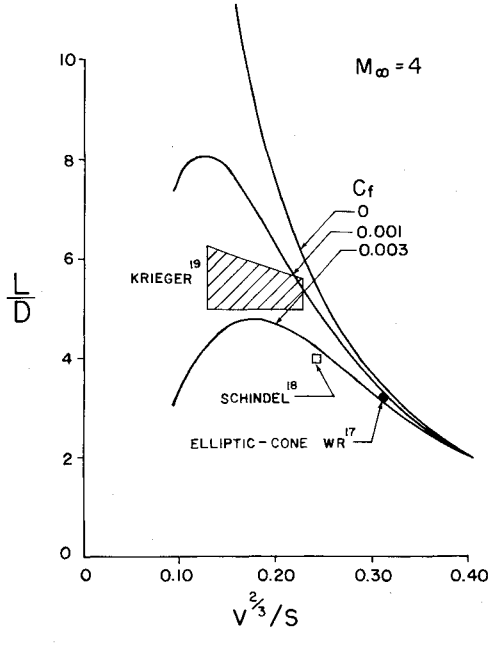

Fig. 15 Effect of friction drag on lift-to-drag ratio.

the volumetric factor $V^{2/3}/S$, in ratio with its counterpart for the idealized cone waverider, is shown in Fig. 12 as a function of ϕ_ℓ for various values of K_δ. For the class A configurations, the ratio $V^{2/3}/S$ is smaller than its counterpart for the idealized cone waverider by less than 10%. The effective slenderness ratio A_b/S is only slightly smaller for all conditions, by at most 3%, than its counterpart for the idealized cone waverider.

Figure 13 shows L/D_w for the fully optimized waveriders as a function of $V^{2/3}/S$ for $M_\infty = 3$, 4, and 5. For a fixed value of $V^{2/3}/S$, the lift-to-drag ratio L/D_w increases as M_∞ increases. The fully optimized waveriders for the class B configurations produce values of L/D_w that are too large for the scale of Fig. 13, and thus the curves represent only class A configurations. A comparison with various other configurations is also shown in Fig. 13. The solid circle data point is the on-design experimental point for $M_\infty = 4$ for the elliptic-cone waverider of Ref. 17. This point agrees well with the fully optimized waverider of the present analysis. The square data point represents the experimental maximum L/D (at $M_\infty = 6$) for the lifting body of Schindel,[18] which produces a smaller L/D than the present optimized waveriders. The shaded trapezoidal area represents the data range of "aerodynamic configured" missiles discussed by Krieger,[19] which also include friction drag in the value of L/D. These configurations have high L/D values, but they are less than the optimized waveriders for the same value of $V^{2/3}/S$, except perhaps in the low Mach number range.

Figure 14 shows L/D_w for the fully optimized waveriders as a function of the effective slenderness ratio A_b/S for $M_\infty = 3$ and 5. For large Mach numbers, this representation is nearly independent of M_∞. Again, the results reflect only the class A configurations, since the results for the class B configurations are off-scale (large L/D). The solid circle data point represents the on-design elliptic-cone waverider of Ref. 17, and it falls slightly under the curves for the present optimized waveriders. The square data point represents the configuration of Schindel, which falls below the curves for the present optimized configurations. The appropriate data for the aerodynamic configured vehicles of Krieger were not available.

Effects of Friction Drag

The viscous or friction drag for the forebody of a waverider can be represented by $D_f \equiv qS_wC_f$, where S_w is the wetted area of the body, given by Eq. (21), and C_f is an appropriate average coefficient of friction. The lift-to-drag ratio can now be written as

$$\frac{L}{D} = \frac{L}{D_w + qS_wC_f} \tag{43}$$

where L and D_w are the lift and wave drag used previously. The value of C_f must be estimated for a given configuration and range of flight conditions. It depends on the Reynolds number, Mach number, laminar or turbulent flow, transition, wall heating, and effects of corner flows. For laminar flow on a flat plate, C_f is approximated by $C_f = 1.328\, f(M_\infty)/\sqrt{Re}$, where $R_e \equiv \rho_\infty V_\infty \ell/\mu_\infty$ is the freestream Reynolds number based on the length, and $f(M_\infty)$ is a function of Mach number depending on the nature of the viscosity-temperature relation, being somewhat less than unity. Based on expressions such as this, modified for conical flow and turbulence, possible values of C_f of interest were taken to lie in the range $0.001 < C_f < 0.003$. Figure 15 is a redrawing of Fig. 13 for $M_\infty = 4$ showing the effects of friction drag using Eq. (43). Figure 15 shows that friction drag becomes more significant the more slender the body, that is, the smaller that δ, $V^{2/3}/S$, and A_b/S become. It can also be seen that there is another optimum for L/D that involves the friction drag, since the curves for nonzero values of C_f show maximum values. The experimental results all contain friction drag, and only the curve for $C_f = 0$ is frictionless.

Concluding Remarks

A study of waverider configurations constructed from axisymmetric flow fields past circular cones has been set forth. The approximate results were analytical and cast in the form of hypersonic small-disturbance theory. Waverider configurations were sought that produced a maximum lift-to-drag ratio subject to a specified constraint. Possible constraint conditions were fixed lift, volume, base area, or projected planform area, but results were presented only for the fixed-lift constraint. Two types of optimized configurations result from the analysis: a pointed-nose configuration with discrete winglets and a circular-cone-segment underbody referred to as class A, and a rounded-nose sharp-lip configuration with a curved concave underbody referred to as class B. For the fully optimized conditions (δ varied), only the class A configurations were possible for $K_\delta \gtrsim 0.17$, which is generally the range of practical interest for lifting bodies. For $K_\delta \lesssim 0.17$, only the class B configurations were possible; these configurations, which were very thin with small volumes and produced very high values of L/D, should possibly be

referred to more appropriately as wings than bodies. A simple analysis for an idealized cone waverider was found to be a good approximation for the class A bodies. Comparison of various results with other types of lifting-body configurations suggests that properly selected waverider configurations are among the best producers of high lift-to-drag ratios.

Acknowledgment

This work was sponsored by the Air Force Armament Laboratory under Contract F08635-80-K-0340.

References

[1]Nonweiler, T.R.F., "Delta Wings of Shape Amenable to Exact Shock-Wave Theory," *Journal of the Royal Aeronautical Society,* Vol. 67, 1963, p. 39.

[2]Jones, J.G. and Woods, P.A., "The Design of Compression Surfaces for High Supersonic Speeds Using Conical Flow Fields," Aeronautical Research Council R&M No. 3539, 1963.

[3]Maikapar, G.I., "Bodies Formed by the Stream Surfaces of Conical Flows," *Fluid Dynamics,* Vol. 1, No. 1, 1966, pp. 89-90, see also, *Mekhanika Zhidkosti i Gaza,* Vol. 1, No. 1, 1966, pp. 126-127.

[4]Seddon, J. and Spence, A., "The Use of Known Flow Fields as an Approach to the Design of High Speed Aircraft," AGARD CP 30, *Hypersonic Boundary Layers and Flow Fields,* London, May 1968.

[5]Cole, J.D. and Zien, T.F., "A Class of Three-Dimensional Optimum Hypersonic Wings," *AIAA Journal,* Vol. 7, Feb. 1969, pp. 264-271.

[6]Küchemann, D., *The Aerodynamic Design of Aircraft,* Pergamon Press, London, 1978, Chap. 8.

[7]Rasmussen, M.L., "Waverider Configurations Derived from Inclined Circular and Elliptic Cones," *Journal of Spacecraft and Rockets,* Vol. 17, Nov.-Dec. 1980, p. 537-545.

[8]Rasmussen, M.L., Daniel, D.C., and Jischke, M.C., "Supersonic Aerodynamics of a Class of Cone-Derived Waveriders," 12th Navy Symposium on Aeroballistics, David W. Taylor Naval Ship Research and Development Center, Bethesda, Md., May 1981.

[9]Lusty, A.H. and Miele, A., "Bodies of Maximum Lift-to-Drag Ratio in Hypersonic Flow," *AIAA Journal,* Vol. 4, Dec. 1966, pp. 2130-2135.

[10]Huang, H-Y., "Variational Approach to Conical Bodies Having Maximum Lift-to-Drag Ratio at Hypersonic Speeds," *Journal of Optimization Theory and Applications,* Vol. 2, No. 5, 1968, pp. 348-362.

[11]Doty, R.T. and Rasmussen, M.L., "Approximation for Hypersonic Flow Past an Inclined Cone," *AIAA Journal,* Vol. 11, Sept. 1973, pp. 1310-1315.

[12]Rasmussen, M.L. and Lee, H.M., "Approximation for Hypersonic Flow Past a Slender Elliptic Cone," AIAA Paper 79-0364, New Orleans, La., Jan. 1979.

[13]Jischke, M.C., "Supersonic Flow Past Conical Bodies with Nearly Circular Cross Sections," *AIAA Journal,* Vol. 19, Feb. 1981, pp. 242-245.

[14]Hildebrand, F.B., *Methods of Applied Mathematics,* 2nd ed., Prentice-Hall, Inc., Englewood Cliffs, N.J., 1965, pp. 141-143.

[15]Weinstock, R., *Calculus of Variations,* Dover Publications, Inc., New York, 1974, Chap. 4.

[16]Broadaway, R., "Aerodynamics of a Simple Cone-Derived Waverider," M.S. Thesis, University of Oklahoma, Norman, Okla., Feb. 1983.

[17]Rasmussen, M.L., Jischke, M.C., and Daniel, D.C., "Experimental Forces and Moments on Cone-Derived Waveriders for $M_\infty = 3$ to 5," *Journal of Spacecraft and Rockets,* Vol. 19, Nov.-Dec. 1982, pp. 592-598.

[18]Schindel, L.H., "Design of High Performance Hypersonic Missiles," AIAA Paper 82-0391, Orlando, Fla., Jan. 1982.

[19]Krieger, R.J., "Summary of Design and Performance Characteristics of Aerodynamic Configured Missiles," AIAA Paper 81-0286, St. Louis, Mo., Jan. 1981.